Chapter 1
eds. T. Gulrez and A. Hassanien
Advances in Robotics and Virtual Reality
Springer-Verlag, 2011

High-field MRI-Compatible Needle Placement Robots for Prostate Interventions: Pneumatic and Piezoelectric Approaches

Hao Su[1], Gregory A. Cole[1] and Gregory S. Fischer[1]

Automation and Interventional Medicine (AIM) Laboratory,
Department of Mechanical Engineering, Worcester Polytechnic Institute,
Worcester, MA, 01609, USA. Phone: (001)508-831-5261,
Email: [haosu,gfischer]@wpi.edu Web: http://aimlab.wpi.edu

Abstract. Magnetic resonance imaging (MRI) can be a very effective imaging modality for live guidance during surgical procedures. The rationale of MRI-guided surgery with robot-assistance is to perform surgical interventions utilizing "real-time" image feedback while minimize operation time and improves the surgical outcomes. However, challenges arise from electromagnetic compatibility within the high-field (1.5 Tesla or greater) MRI environment and mechanical constraints due to the confined close-bore space. This chapter presents two distinct MRI-compatible approaches for image-guided transperineal prostate needle placement. It articulates the robotic mechanism, actuator and sensor design, controller design and system integration for a pneumatically actuated robotic needle guide and a piezoelectrically actuated needle placement system. The two degree-of-freedom (DOF) pneumatic robot with manual needle insertion has a signal to noise ratio (SNR) loss limited to 5% with alignment accuracy under servo pneumatic control better than $0.94mm$ per axis. While the 6-DOF piezoelectrically actuated robot is the first demonstration of a novel multi piezoelectric actuator drive with less than 2% SNR loss for high-field MRI operating at full speed during imaging. Preliminary experiments in phantom studies evaluate system MRI compatibility, workflow, visualization and targeting accuracy.

1 Introduction

Prostate cancer is the most common cancer in males and the second most commonly found cancer in human. The estimated new prostate cancer cases (192,280) in 2009 account for 25% incident cases in men in the United States [25]. Each year approximately 1.5 million core needle biopsies are performed, yielding about 220,000 new prostate cancer cases. Over 40,000 brachytherapy radioactive seed implantation procedures are performed in the United States each year, and the number is steadily rising. Prostate specific antigen blood tests and digital rectal exams are the two major preliminary prostate cancer diagnosis methods. However, prostate biopsy is

the conclusive approach to confirm cancer diagnosis. Prostate brachytherapy and cryotherapy are often used for early treatment.

Magnetic resonance imaging can provide high resolution multi-parametric imaging, large soft tissue contrast, and interactive image updates making it an ideal guidance modality for needle-based prostate interventions. In this chapter, two MRI-compatible robotic assistants utilizing pneumatic and piezoelectric actuation for needle placement are designed for image-guided prostate interventions. Both systems are intended to provide increased positioning accuracy through the use of precision motion and image feedback. The actuated systems enable acquisition of interactively updated images during robot motion in situ. These images enable real-time guidance and of needle tracking in MRI which may be used for image-guided closed loop control of needle placement.

The motivation of deploying robotic system in prostate interventions comes from three major aspects. First, robot-assisted surgery guarantees good geometric accuracy as it relies upon rigid mechanical structures and motion/force control of the robot, thus overcoming the accuracy limits of traditional mechanical templates ($5mm$) and allowing needle angulation. Second, robots can be designed with appropriate scale to fit into open scanner bores or cylindrical closed-bores. Third, since robots are stable and untiring, they can stay inside the scanner bore and perform interventional procedures via teleoperated control more easily than human surgeons. This eliminates or reduces the necessity of the iterative and time-consuming procedure that usually takes several cycles of imaging for registration inside bore, interventions out of bore (due to space limit) and confirmation inside bore. In general, MRI-guided surgery with robot-assistance can ultimately minimize operation time and maximize placement accuracy thus improves the surgical outcomes. Moreover, it can greatly reduce the equipment cost and overhead.

Contents of the Chapter: This chapter is organized as follows: After a thorough literature review in Section2, Section 3 analyzes and articulates the design requirement. Section 4 describes the 2-DOF pneumatic needle placement robot design with manual insertion and Section 5 describes the 6-DOF fully actuated needle placement robot design with piezoelectric actuation. Section 6 presents the system architecture and workflow utilizing these two robots. A number of experiments in 3 Tesla closed-bore scanner and analysis are elaborated in Section 7. Finally, a discussion of the system is presented in Section 8 that summarizes the experimental insight and future work.

2 Background and Literature Review

Transrectal ultrasound (TRUS) is the current "gold standard" for guiding both biopsy and brachytherapy due to its real-time nature, low cost and ease of use. Fig. 1 shows the traditional template-based TRUS-guided approach to brachytherapy seed placement. However, TRUS-guided biopsy has a detection rate of only $20-30\%$ [48]. The low success rate is largely due to the inherent limitation of ultrasound imaging itself and the mechanical template used in the procedure to guide the needles. Ultrasound imaging is inferior to MRI for prostate cancer treatment due to its limited resolution and inability to display implanted radiation seeds. Furthermore, the ultrasound probe deforms the prostate and can induce seed migration. Since the dosimetry plan is usually performed on the manual segmentation of pre-operative

ultrasound images, the seed placement accuracy is deteriorated because of the low image quality and probe induced tissue deformation. On the other hand, the template used to guide needles in TRUS is a $6cm \times 6cm$ mechanical grid with $5mm \times 5mm$ space distance which limits the entrance location at the perineum and the positioning resolution of needle insertion. In addition, this mechanically constrained template limits the ability for needle angulation to adjust needle orientation for better targeting or to avoid pubic arch interference (PAI), thus restricting the eligible patient population.

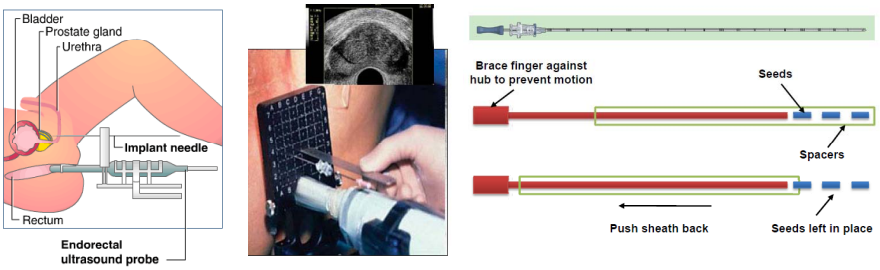

Fig. 1. Traditional template-based TRUS-guided approach to prostate brachytherapy (left and middle). Brachytherapy needle from CP Medical and the schematic procedure of preloaded needles: after insertion, the sheath is withdrawn over the stylet, leaving the seeds in the place (modified from [52]) (right).

Conversely, the MRI-based medical paradigm offers several advantages over other imaging counterparts. First, MRI has multiple mechanisms to provide high-fidelity soft tissue contrast and spatial resolution. Second, MRI is a three-dimensional imaging modality that permits arbitrary imaging plane selection, even in a dynamic manner. Third, MRI does not produce ionizing radiation thus imposes no radiation safety hazard to the patient or practitioner. The clinical efficacy of MRI-guided prostate brachytherapy and biopsy was demonstrated by D'Amico et al. at the Brigham and Women's Hospital using a 0.5T open-MRI scanner [10]. MR images were used to plan and monitor transperineal needle placement. The needles were inserted manually using a guide comprising a grid of holes, with the patient in the lithotomy position, similarly to the TRUS-guided approach.

The challenges, however, arise from electromagnetic compatibility in the high-field (1.5T or greater) MRI environment and mechanical constraints due to the confined closed-bore space. The bidirectional MRI compatibility means that both the device does not disturb the scanner function (which may cause image artifacts)and the scanner should not disturb the device functionality. Thus, in the actuation level, conventional DC/AC motors that reply on electromagnetism for conventional robotic actuation is not feasible in MRI. In the material level, conductive materials such as metallic components can induce heating thus special means should be taken to avoid the side-effects of these materials or even avoid using them. Moreover, the

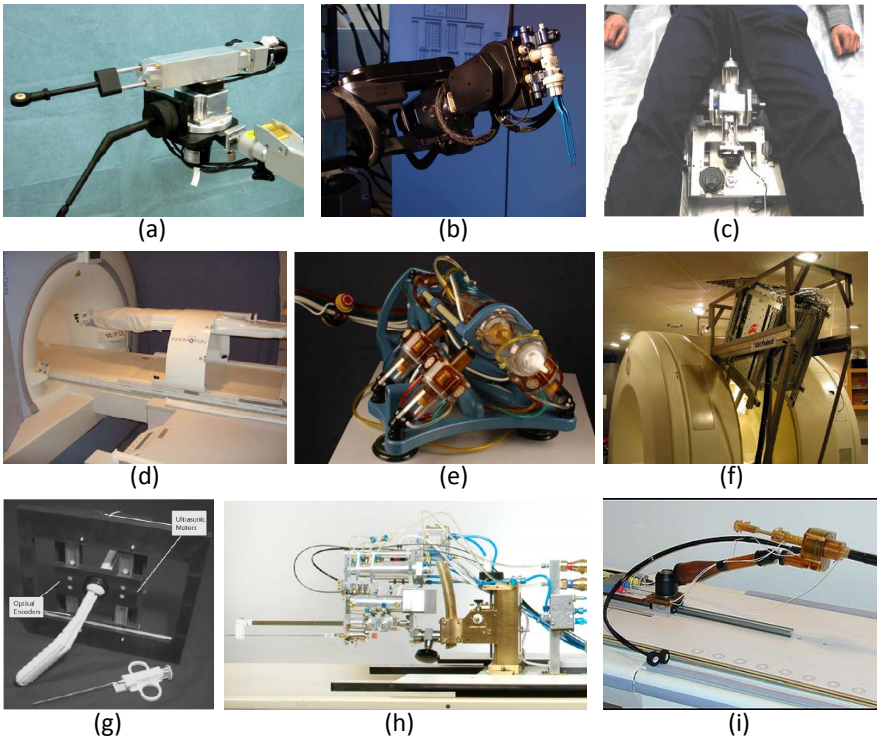

Fig. 2. MRI guided robots and assistance device: Masamune et al. [31] (a), Sutherland et al. [46](b), Goldenberg et al. [21] (c), INNOMOTION [32] (d), Stoianovici et al. (e), Chinzei et al. [7] (f), Elhawary et al. [13] (g), van den Bosch et al. [5] (h) and Krieger et al. [27] (i).

confined physical space in closed-bore high-field MRI presents stringent challenges for mechanical design.

Thorough reviews of MRI-compatible systems to date for image-guided interventions are presented by Tsekos, et al. [51] and Elhawary, et al. [12]. The potential role of robotics in MRI-guided prostate interventions was thoroughly discussed in [18] and a clinical overview of MRI-guided biopsy of the prostate is presented in [34]. Fig. 2 shows a collection of the MRI-compatible assistants for prostate interventions developed to date. Robotic assistance has been investigated for guiding instrument placement in MRI, beginning with neurosurgery [31]. A most recent MRI-guided neurosurgical robot [46] was developed by Sutherland et. al. Goldenberg et al. [21] proposed an MRI-compatible robotic system for image-guided prostatic interventions. INNOMOTION [32] is the first commercially available MRI-guided robot that utilizes pneumatic actuation and was recently acquired by Synthes©. Stoianovici et al. [38] described a MRI-compatible pneumatic stepper motor PneuStep, which has a very low level of image interference. Chinzei et al. [7] developed a general-purpose robotic assistant for open MRI that was subsequently adapted for transperineal intraprostatic needle placement [11]. Elhawary et al. [13] performed transrectal

prostate biopsy. van den Bosch et al. [5] performed MRI-guided needle placement and seed delivery in the prostate. Krieger et al. [27] presented a 2-DOF passive, unencoded, and manually manipulated mechanical linkage to aim a needle guide for transrectal prostate biopsy with MRI guidance. Song et. al [37] presented a pneumatic robot for MRI-guided transperineal prostate biopsy and brachytherapy. Two recent developments of pneumatically actuated robots [5, 35] further investigated the actuation feasibility in terms of compatibility and accuracy. The last decade also witnessed the development of MRI-guided robots for other surgical applications, including cardiac surgery [29, 30, 57] and breast cancer diagnosis [56], etc.

Generally, there are four actuation principles utilized in MRI applications, namely remote actuation, hydraulic, pneumatic and ultrasonic/piezoelectric actuators [20]. A substantial armamentarium of actuation methods has been studied in a number of image-guided interventions and rehabilitation scenarios. Early MRI-compatible robotic systems focus on manual driven or ultrasonic motor driven and the latter cannot run during imaging due to significant signal loss. Remote actuation suffers from bulky structure, low bandwidth and lower resolution and is not preferable for robotic applications. Hydraulic and pneumatic actuation are considered as the silver bullet for MRI applications in the sense that these system can completely avoid electrical and magnetic noise inside the scanner by using dielectric materials, thus providing high signal noise ratio. Hydraulic systems render very large output force, but usually suffer from cavitation and fluid leakage. Pneumatic actuation is easier to maintain but is back-drivable due to the compressibility of air and is more favorable for high bandwidth applications, especially ideal for force control. The disadvantages of pneumatic actuation is also because of compressibility of air and the induced time delay, that makes it difficult to control at the millimeter level in which medical robotics usually tries to maintain. Ultrasonic/piezoelectric actuation provides high positioning resolution [23,24] and does not rely upon magnetism, but since there is still high frequency electrical signal and the piezoelectric elements are often embedded inside ferromagnetic or paramagnetic materials, piezoceramic motors using commercially available motor controllers have been evaluated by [13] which negatively impacted image quality. The difficulty arises from the actuator driving controller that usually induces significant image artifact when utilizing off-the-shelf control circuits. However, the scalability, simplicity, size and inherent robustness of electromechanical systems present a clear advantage over pneumatically actuated systems.

Objective and Contributions: *Generally, no prior work has considered the exploitation of modular robotic systems for in-situ needle placement in high-field closed-bore MRI, with its many merits, in a transperineal manner which alleviates the requirement to perform the implant procedures in a different pose than used for preoperative imaging.* This paper reviews the design of two approaches that comply with the compatibility while address *in-situ* needle placement with reduced cost and system complexity. By leveraging the pneumatic and piezoelectric actuation approaches, the underlying philosophy of this research effort aims to explore the two distinct methods to demonstrate two design examples that provide semi-automatic and teleoperated needle placement robots for prostate interventions respectively. Even the focus of the design targets prostate cancer, this interventional system is possible to be adopted for other percutaneous applications.

3 Design Requirement

3.1 Surgical Procedure Analysis and Design Implication

Robotic design starts from the surgical procedure analysis which provides the guideline and "optimal" solution of designing clinically practical robots. This includes the analysis of prostatic intervention classification based on interventional approach (transrectal, transperineal and transurinal) and the motion analysis of needle insertion during biopsy, brachytherapy and ablation.

The transperineal approach is preferable for the following reasons [3]. First, transrectal approach samples the peripheral zone (the most common location of the cancer) across its smallest dimension and has a higher possibility of missing the cancer than the transperineal approach. Second, the transrectal method does not allow accessing some regions of the prostate that are blocked by the urethra. Third, the transrectal technique is not extendible to therapy (brachytherapy or cryotherapy) which requires multiple needle placements because of increased rectal injury that has a high risk of infection.

As shown in Fig. 1 right, the clinical 18Gauge (1.27mm) needles for prostate brachytherapy have an inner stylet and hollow sheath. Radioactive seeds are preloaded with 5.5mm spacers between them before staring the surgery. During the insertion, one hand holds the cannula and the other hand brace against stylet hub to prevent relative motion. After insertion, the sheath is withdrawn over the stylet while leaving the seeds in place. To mimic the physician preload needle type brachytherapy procedure, the needle driver provides 1-DOF cannula rotation about its axis with 1-DOF translational insertion. Another 1-DOF of translational stylet motion is implemented to coordinate the motion with respect to the cannula. The rotation motion of the cannula may be used for bevel-based steering to limit deflection or may be used for active cannula operation [55].

3.2 System Requirement

The system's principal function is accurate transperineal needle placement in the prostate for diagnosis and treatment, primarily in the form of biopsy and brachytherapy seed placement, respectively. The patient is positioned in the supine position with the legs spread and raised as shown in Fig. 3 (left). The patient is in a similar configuration to that of TRUS-guided brachytherapy, but the typical MRI bore's constraint ($\leq$ 60cm diameter) necessitates reducing the spread of the legs and lowering the knees into a semi-lithotomy position. The robot operates in the confined space between the patient's legs without interference with the patient, MRI scanner components, anesthesia equipment, and auxiliary equipment present as shown in the cross-section shown in Fig. 3 (right).

The size of an average prostate is $50mm$ in the lateral direction by $35mm$ in the anterior-posterior direction by $40mm$ in length. The average prostate volume is about 35cc; by the end of a procedure, this volume enlarges by as much as 25% due to swelling [52]. For our system, the standard $60mm \times 60mm$ perineal window of TRUS-guided brachytherapy was increased to $100mm \times 100mm$, in order to accommodate patient variability and lateral asymmetries in patient setup. In depth, the workspace extends to $150mm$ superior of the perineal surface. Direct access to

all clinically relevant locations in the prostate is not always possible with a needle inserted purely along apex-base direction due to PAI. Needle angulation in the sagittal and coronal planes will enable procedure to be performed on many of these patients where brachytherapy is typically contraindicated due to PAI as described by Fu, et al. [17].

The robot is mounted to a manual linear slide that positions the robot in the access tunnel and allows fast removal for reloading brachytherapy needles or collecting harvested biopsy tissue. The primary actuated motions of the robot include two prismatic motions which replicate the DOF of a traditional template-base approach, and two rotational motions for aligning the needle axis to help avoid PAI and critical structures. In addition to these base motions, application-specific motions are also required; these include needle insertion, cannula retraction or biopsy gun actuation, and needle rotation. The accuracy of the individual servo-controlled joints is targeted to be 0.1mm, and the needle placement accuracy of the robotic system itself is targeted to be better than 1.0mm. This target accuracy approximates the voxel size of the MR images used which represents the finest possible targeting precision. The overall system accuracy, however, is expected to be somewhat less when effects such as imaging resolution, needle deflection, and tissue deformation are taken into account. The MR image resolution is typically 1mm and the clinically significant target is typically $5mm$ in size (the precision of a traditional TRUS template).

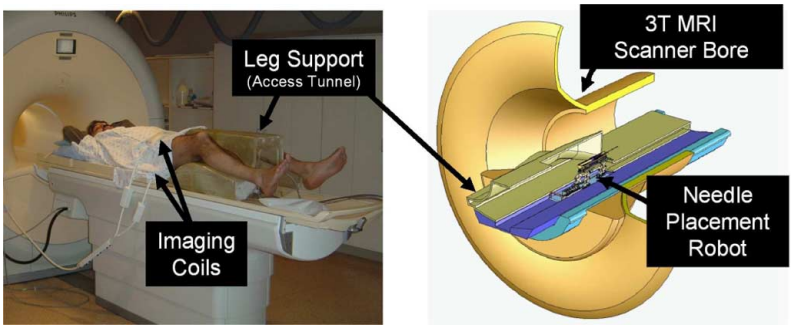

Fig. 3. Positioning of the patient in the semilithotomy position on the leg support (left). The robot accesses the prostate through the perineal wall, which rests against the superior surface of the tunnel within the leg rest (right). [15] ©2008 IEEE

3.3 MRI Compatibility Requirements

Significant complexity is introduced when designing a system operating inside the bore of high-field 1.5-3T MRI scanners since traditional mechatronics materials, sensors and actuators cannot be employed. This section addresses the additional system requirements arising from compatibility with the MRI scanner. A thorough description of the issues relating to MR Safety is described by Shellock [36]. The MR-Safe definitions are according to the ASTM Standard F2052 [1] while MR-compatible is the commonly used term:

MR-Safe: The device, when used in the MR environment, has been demonstrated to present no additional risk to the patient or other individual, but may affect the quality of the diagnostic information. The MR conditions in which the device was tested should be specified in conjunction with the term MR safe since a device that is safe under one set of conditions may not be found to be so under more extreme MR conditions.

MR-Compatible: A device is considered MR-compatible if it is MR safe and if it, when used in the MR environment, has been demonstrated to neither significantly affect the quality of the diagnostic information nor have its operations affected by the MR device. The MR conditions in which the device was tested should be specified in conjunction with the term MR-compatible since a device that is safe under one set of conditions may not be found to be so under more extreme MR conditions.

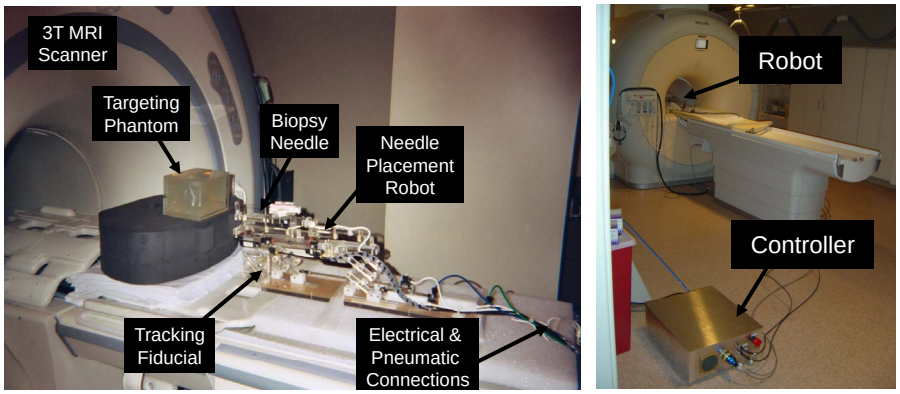

Fig. 4. Pneumatic robotic needle placement mechanism with two active DOF and one passive, encoded needle insertion. Dynamic global registration is achieved with the attached tracking fiducial (left). The configuration of the robot with the controller in the scanner room (right). [15] ©2008 IEEE

4 Needle Placement Robot: Pneumatic Approach

The first iteration of a pneumatic system [15] provides the two prismatic motions in the axial plane over the perineum and an encoded manual needle guide, as shown in shown in Fig. 4. This represents an automated high-resolution needle guide, functionally similar to the template used in conventional brachytherapy. The primary base DOFs are broken into two decoupled planar motions. Motion in the vertical plane is based on a modified version of a scissor lift mechanism that is traditionally used for plane parallel motion. Motion in the horizontal plane is accomplished with a second planar bar mechanism. The base of the manipulator has a modular platform that allows for different end effectors to be mounted on it. The two initial end effectors will accommodate biopsy guns and brachytherapy needles. Both require an insertion phase; the former requires activating a single-acting button to engage the

device and a safety lock. The latter requires an additional controlled linear motion to accommodate the cannula retraction to release brachytherapy seeds. Rotation of the needle about its axis may be implemented to either "drill" the needle in to limit deflection, or to steer the needle using bevel steering techniques such as those described in [55]. Sterility has been taken into consideration for the design of the end effectors. In particular, the portion of the manipulator and leg rest that is in direct contact with the patient or needle will be removable and made of materials that are suitable for sterilization. The remainder of the robot will be draped. An alternative solution is to enclose the entire leg rest with the robot in a sterile drape, thus completely isolating the robot from the patient except for the needle.

4.1 Mechanical Design

Mechanism design is particularly important since the robot is non-metallic and must operate in a confined space. The design was developed such that the kinematics can be simplified, control can be made less complex, motions may be decoupled, actuators can be aligned appropriately, and system rigidity can be increased. Based upon analysis of the workspace and the application, the following additional design requirements have been adopted: 1) prismatic base motions should be able to be decoupled from angulation since the majority of procedures will not require the two rotational DOFs; 2) actuator motion should be in the axial direction (aligned with the scanner's axis) to maintain a compact profile; and 3) extension in both the vertical and horizontal planes should be telescopic to minimize the working envelope.

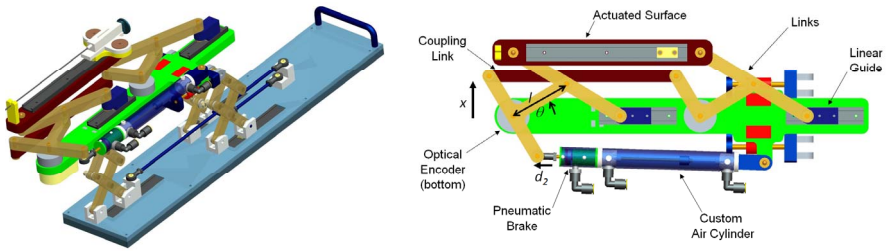

Fig. 5. This mechanism provides for motion in the vertical plane. Coupling the forward and rear motion provides for vertical travel, independently moving the rear provides for elevation angle adjustment (left). This mechanism provides for motion in the horizontal plane. The design shown provides prismatic motion only; rotation can be enabled by actuating rear motion independently by replacing coupling link (L_c) with a second actuator. The modular, encoded needle guide senses the depth during manual needle insertion and can be replaced with different end effectors for other procedures (right).

The primary base DOFs are broken into two decoupled planar motions. Motion in the vertical plane includes 100 mm of vertical travel, and optionally up to 15° of elevation angle. This is achieved using a modified version of a scissor lift mechanism that is traditionally used for planar parallel motion. By coupling two such

mechanisms, as shown in Fig. 5 (left), 2-DOF motion can be achieved. Stability is increased by using a pair of such mechanisms in the rear. For purely prismatic motion, both slides move in unison; angulation is generated by relative motions. To aid in decoupling, the actuator for the rear slide can be fixed to the carriage of the primary motion linear drive, thus allowing one actuator to be locked when angulation is unnecessary. As shown in Fig. 5 (left), the push rods for the front and rear motions are coupled together to maintain only translational motion in the current prototype.

Motion in the horizontal plane is accomplished with a second planar bar mechanism. This motion is achieved by coupling two straight line motion mechanisms, as shown in Fig. 5 (right), generally referred to as Scott-Russell mechanisms. By combining two such straight-line motions, both linear and rotational motions can be realized in the horizontal plane. The choice of this design over the use of the previously described scissor-type mechanism is that this allows for bilateral motion with respect to the nominal center position. Fig. 5 (right) shows the mechanism where only translation is available; this is accomplished by linking the front and rear mechanisms with a connecting bar. A benefit of this design is that it is straightforward to add the rotational motion for future designs by replacing the rigid connecting bar (L_c) with another actuator. Due to the relative ease of manufacturing, the current iteration of the system is made primarily out of acrylic. In future design iterations, the links will be made out of high strength, dimensionally stable, highly electrically insulating, and sterilizable plastic (e.g., Ultem or polyetheretherketone (PEEK)).

4.2 Pneumatic Actuator Design

The MRI environment places severe restrictions on the choice of sensors and actuators. Many mechatronic systems use electrodynamic actuation, however, the very nature of an electric motor precludes its use in high-field magnetic environments. Therefore, it is necessary to either use actuators that are compatible with the MR environment, or to use a transmission to mechanically couple the manipulator in close proximity to the scanner to standard actuators situated outside the high field. MR-compatible actuators such as piezoceramic motors have been evaluated in [13, 47]; however, these are prone to introducing noise into MR imaging, and therefore, negatively impacting image quality. Mechanical coupling can take the form of flexible drive shafts [27], push-pull cables, or hydraulic (or pneumatic) couplings [19].

Pneumatic cylinders are the actuators of choice for this robot. Accurate servo control of pneumatic actuators using sliding mode control (SMC) with sub-millimeter tracking accuracy and 0.01mm steady-state error (SSE) have been demonstrated in [4]. Although pneumatic actuation seems ideal for MRI, most standard pneumatic cylinders are not suitable for use in MRI. Custom MR compatible pneumatic cylinders have been developed for use with this robot. The design of these cylinders is based upon Airpel 9.3 mm bore cylinders. These cylinders were chosen because the cylinder bore is made of glass and the piston and seals are made of graphite, giving them inherently low friction and MR compatibility. In collaboration with the manufacturer, we developed the cylinder shown in Fig. 5 (right) bottom that are entirely nonmetallic except for the brass shaft. The cylinders can handle up to 100 psi (6.9 bar), and therefore, can apply forces up to 46.8 N. Our newly developed SMC controller has shown sub-millimeter tracking accuracy using this pneumatic actuator [54].

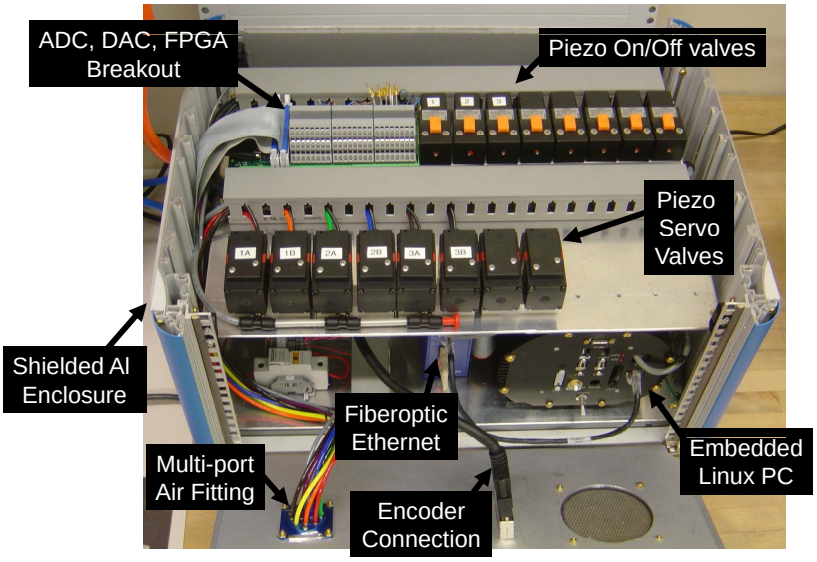

Fig. 6. Controller contains the embedded Linux PC providing low-level servo control, the piezoelectric valves, and the fiber-optic Ethernet converter. The EMI shielded enclosure is placed inside the scanner room near the foot of the bed. Connections to the robot include the multi-tube air hose and the encoder cable; connection to the planning workstation is via fiber-optic Ethernet. [15] ©2008 IEEE

In addition to moving the robot, it is important to be able to lock it in position to provide a stable needle insertion platform. Pneumatically operated, MR-compatible brakes have been developed for this purpose. The brakes are compact units that attach to the ends of the previously described cylinders, as shown in Fig. 5 (right) top, and clamp down on the rod. The design is such that the fail-safe state is locked and applied air pressure releases a spring-loaded collet to enable motion. The brakes are disabled when the axis is being aligned and applied when the needle is to be inserted or an emergency situation arises.

Proportional pressure regulators are implemented for this robot because they allow for direct control of air pressure, thus the force applied by the pneumatic cylinder. This is an advantage because it aids in controller design and also has the inherent safety of being able to limit applied pressure to a prescribed amount. Most pneumatic valves are operated by a solenoid coil; unfortunately, as with electric motors, the very nature of a solenoid coil is a contraindication for its use in an MR environment. With pneumatic control, it is essential to limit the distance from the valve to the cylinder on the robot; thus, it is important to use valves that are safe and effective in the MR environment. By placing the controller in the scanner room near the foot of the bed, air tubing lengths are reduced to 5 m. The robot controller uses piezoelectrically actuated proportional pressure valves, thus permitting their use near MRI. A pair of these valves provide a differential pressure of $\pm$ 100 psi

on the cylinder piston for each actuated axis. A further benefit of piezoelectrically actuated valves is the rapid response time (4 ms). Thus, by using piezoelectric valves, the robot's bandwidth can be increased significantly by limiting tubing lengths and increasing controller update rate.

4.3 Robot Controller Hardware

MRI is very sensitive to electrical signals passing in and out of the scanner room. Electrical cables passing through the patch panel or wave guide can act as antennas, bringing stray RF noise into the scanner room. For that reason, and to minimize the distance between the valves and the robot, the robot controller is placed inside the scanner room. The controller comprises an electromagnetic interference (EMI) shielded enclosure that sits at the foot of the scanner bed, as shown in Fig. 4 right; the controller has proved to be able to operate $3m$ from the edge of the scanner bore. Inside of the enclosure is an embedded computer with analog I/O for interfacing with valves and pressure sensors and a field programmable gate array (FPGA) module for interfacing with joint encoders (see Fig. 6). Also, in the enclosure are the piezoelectric servo valves, piezoelectric brake valves, and pressure sensors. The distance between the servo valves and the robot is minimized to less than $5m$, thus maximizing the bandwidth of the pneumatic actuators. Control software on the embedded PC provides for low-level joint control and an interface to interactive scripting and higher level trajectory planning. Communication between the low-level control PC and the planning and control workstation sitting in the MR console room is through a 100-FX fiber-optic Ethernet connection. In the prototype system, power is supplied to the controller from a filtered dc power supply that passes through the patch panel; a commercially available MR-compatible power supply will be used in future design iterations. No other electrical connections pass out of the scanner room, thus significantly limiting the MR imaging interference.

5 Needle Placement Robot: Piezoelectric Approach

The newly developed piezoelectric robot [16, 40, 42–44], shown in Fig. 7, offers the capability of real-time *in-situ* needle steering in high-field MRI. It consists of a modular 3-DOF needle driver with optical tracking frame coupled similar to that of the pneumatic robot. The modular needle driver simultaneously provides needle cannula rotation and independent cannula and stylet prismatic motion. For experimental purposes, it is shown with a generic MRI-compatible 3-DOF $x-y-z$ stage; however, application specific designs will be used for the appropriate clinical applications. The piezoelectric motors are actuated using custom motor control drive circuits integrated into a controller architecture adapted from that of the pneumatic robot. To overcome the loss of needle tip proprioception information, a multi-DOF fiber optic force sensor is integrated with the piezoelectric robot.

The needle placement robot consists of a needle driver module (3-DOF) and Cartesian positioning module (3-DOF). The material is rapid prototyped with ABS and laser cut acrylic. Considering the supine configuration and the robot workspace, the width of the robot is limited to 6cm. As shown in Fig. 7 (left), the lower layer of the needle driver module is driven with linear piezoelectric motor and the upper layer provides cannula rotation motion and stylet prismatic motion.

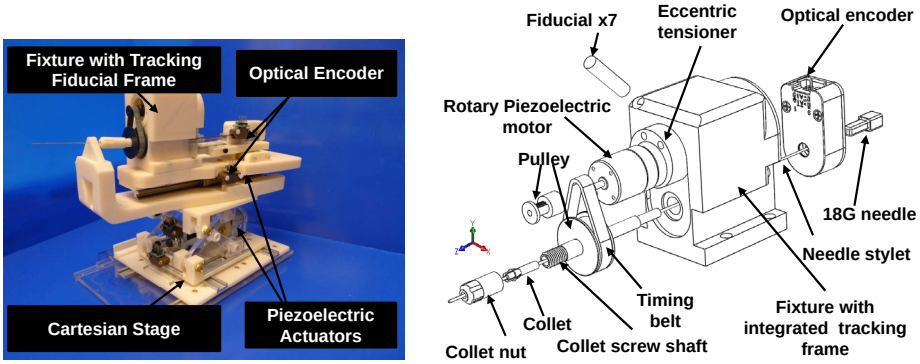

Fig. 7. Piezoelectric robotic needle placement mechanism with three DOF needle rotation and collinear translation for prostate brachytherapy on a three DOF Cartesian stage (left). Detailed design of the needle driver platform (right). [44] ©2011 IEEE

5.1 Mechanical Design

To design a needle driver that allows a large variety of standard needles, a new clamping device shown in Fig. 7 (right) rigidly connects the needle shaft to the driving motor mechanism. This structure is a collet mechanism and a hollow screw made of stereolithography ABS is twisted to fasten the collet thus rigidly locking the needle shaft on the clamping device. The clamping device is connected to the rotary motor through a timing belt that can be fastened by an eccentric belt tensioner. The clamping device is generic in the sense that we have designed 3 sets of collets and each collet can accommodate a width range of needle diameters. The overall needle diameter range is from 25 Gauge to 7 Gauge. By this token, it can not only fasten brachytherapy needle, but also biopsy needles and most other standard needles instead of designing some specific structure to hold the needle handle.

Once a preloaded needle or biopsy gun is inserted, the collet can rigidly clamp the cannula shaft. Since the linear motor is collinear with the collet and shaft, we need to offset the shaft to manually load the needle. We designed a brass spring preloaded mechanism that provides lateral passive motion freedom. The operator can squeeze the mechanism and offset the top motor fixture then insert the loaded needle through plain bearing housing and finally lock with the needle clamping. This structure allows for easy, reliable and rapid loading and unloading of standard needles.

5.2 Piezoelectric Actuator Driver

The piezoelectric actuators (PiezoMotor, Uppsala, Sweden) chosen are non-harmonic piezoelectric motors which have two advantages over a harmonic drive: the noise caused by the driving wave is much easier to suppress, and the motion produced by the motors is generally at a more desirable speed and torque relative to harmonic piezoelectric motors. Even though piezoelectric motors do not generate magnetic

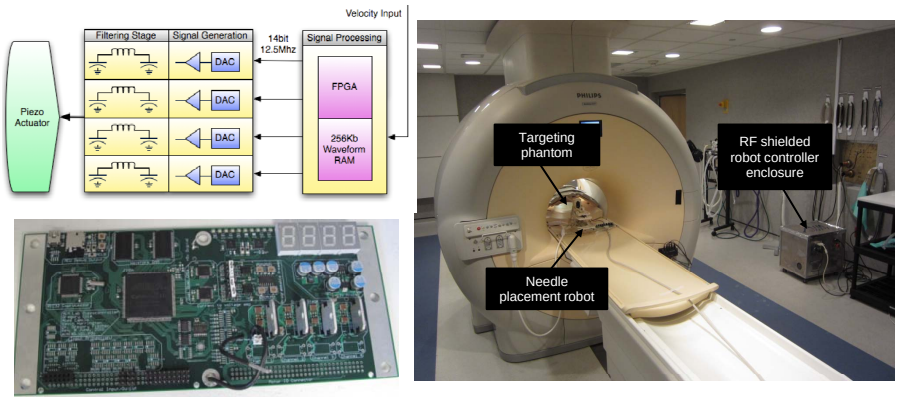

Fig. 8. Piezoelectric actuator driver architecture and prototype using FPGA generated waveform (left), and the configuration of the robot with the controller in the scanner room (right).

fields, commercial motor driver boards usually induce significant image artifacts due to electrical noise according to the most recent result [26]. A new low noise driver [8,9] was developed and its architecture is shown in Fig. 8(left) and Fig. 8 (right) shows the configuration of the robot with the controller in the scanner room. Waveform tables are stored in RAM and utilized by a synthesizer running on the FPGA to generate four independent control waveforms of arbitrary phase and frequency. These control waveforms are then streamed out to the analog amplification stage at 25 mega samples per second.

6 Surgical Visualization and Workflow

6.1 Surgical Visualization

The user interface for the robot is based on 3D Slicer open-source surgical navigation software (3D Slicer Software, http://www.slicer.org). The navigation software runs on a Linux-based workstation in the scanner's console room, and communicates to the robot controller over a fiberoptic connection. A customized graphical user interface (GUI) specially designed for the prostate intervention with the robot is described in [33]. The interface allows smooth operation of the system throughout the clinical workflow including registration, planning, targeting, monitoring and verification (Fig. 9). The workstation is connected to the robot and the scanner's console via Ethernet. OpenIGT Link [49], is used to exchange various types of data including control commands, position data, and images among the components. Fig. 10 shows the configuration used in the system as described in [50].

In the planning phase, pre-operative images are retrieved from a DICOM server and loaded into the navigation software. Registration is performed between the pre-operative planning images and intra-operative imaging using techniques such as those described by Haker, et al. [22]. Target points for the needle insertion are

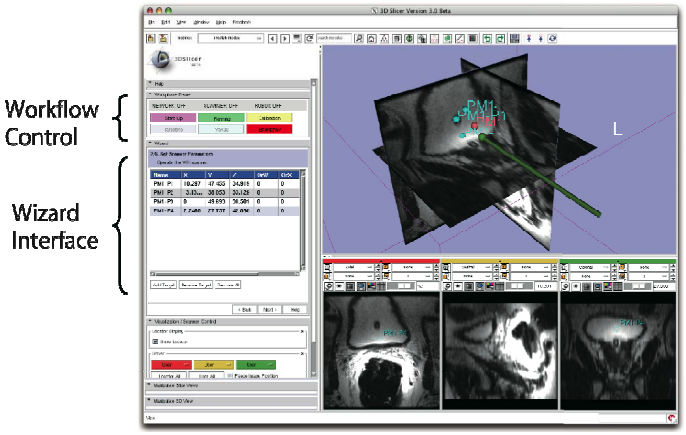

Fig. 9. 3D Slicer planning workstation showing a selected target and the real-time readout of the robot's needle position. The line represents a projection along the needle axis and the sphere represents the location of the needle tip. [15] ©2008 IEEE

selected according to the pre-operative imaging, and the coordinates of the determined target points are selected in the planning GUI. Once the patient and the robot are placed in the MRI scanner, a 2D image of the fiducial frame is acquired and passed to the navigation software to calculate the 6-DOF pose of the robot base for the robot-image registration. The position and orientation of the robot base is sent through the network from the navigation software to the robot controller. After the registration phase, the robot can accept target coordinates represented in the image (patient) coordinate system in standard Right-Anterior-Superior (RAS) coordinates.

During the procedure, a target and an entry point are chosen on the navigation software, and the robot sends the coordinates then aligns the needle guide appropriately. In the current system, the needle is inserted manually while the needle position is monitored by an encoded needle guide and displayed in real-time on the display. Needle advancement in the tissue is visualized on the navigation software in two complementary ways: 1) a 3D view of needle model combined with pre-operative 3D image re-sliced in planes intersecting the needle axis, and 2) 2D real-time MR images acquired from the planes along or perpendicular to the needle path and continuously transferred from the scanner through the network. The former provides a high refresh rate, allowing a clinician to manipulate the needle interactively. The latter provides the changing shape or position of the target lesion with relatively slower rate depending on the imaging speed (typically 0.5Hz).

The interface software enables "closed-loop" needle guidance, where the action made by the robot is captured by the MR imaging, and immediately fed back to a physician to aid their decision for the next action. The reason for keeping a human in the loop is to increase the safety of the needle insertion, and to allow for monitoring progress via live MR images. Once the needle is fully aligned before patient contact, the placement is adjusted in response to the MR images. The physician performs

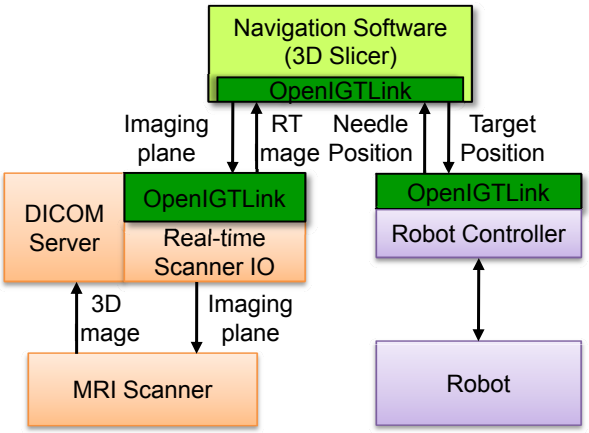

Fig. 10. Diagram shows the connection and the data flow among the robot components. OpenIGTLink, an open-source device communication tool, is used to exchange control, position, and image data.

the insertion under real-time imaging. Fig. 9 shows the planning software with an MR image of the phantom loaded and real-time feedback of the robot position is used to generate the overlaid needle axis model.

6.2 Needle Placement Robot Tracking and Localization

Dynamic global registration between the robot and scanner is achieved by passive tracking the fiducial frame in front of the robot as shown in Fig. 7 (right). The rigid structure of the fiducial frame is made of ABS and seven MR Spot fiducials (Beekley, Bristol, CT) are embedded in the frame to form a Z shape passive fiducial. Any arbitrary MR image slicing through all of the fiducial rods provides the full 6-DOF pose of the frame, and thus the robot, with respect to the scanner. Thus, by locating the fiducial attached to the robot, the transformation between patient coordinates (where planning is performed) and the robot is known. To enhance the system reliability and robustness, multiple slices of fiducial images are used to register robot position using principal component analysis method. The end effector location is then calculated from the kinematics based on the encoder positions.

6.3 System Workflow

The workflow of the system mimics that of traditional TRUS-guided prostate needle insertions, and are as follows (shown in Fig. 11):

1. Acquire pre-procedural MRI volume of the patient's prostate and surrounding anatomy.

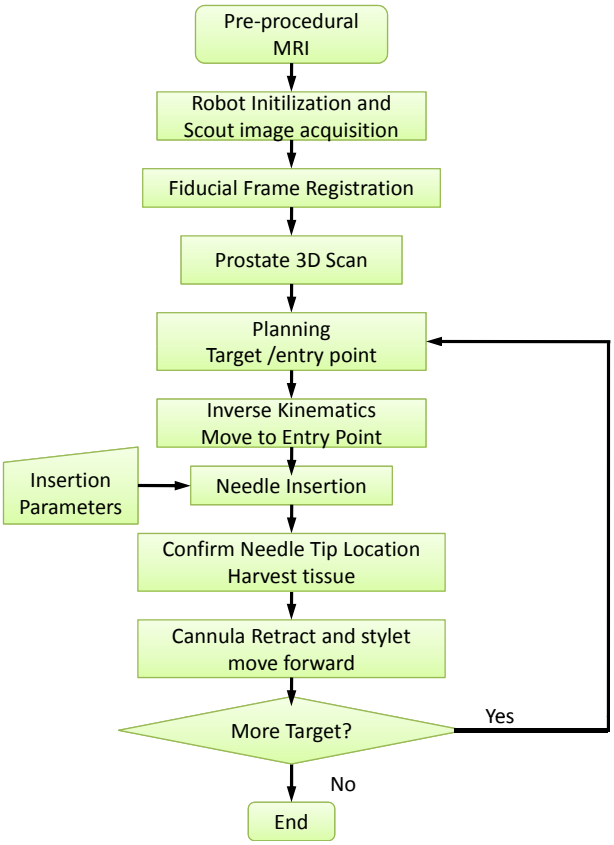

Fig. 11. Workfow of MRI-guided needle placement that mimics that of traditional TRUS-guided prostate needle intervention.

2. Select specific needle tip targets as shown in Fig. 9.
3. Define corresponding needle trajectories.
4. Acquire an MR image of the robot's tracking fiducial.
5. Register the robotic system to patient/scanner coordinates.
6. Load the biopsy needle or pre-loaded brachytherapy needle into the robot's needle driver.
7. Send coordinates in patient coordinates to the robot.
8. Automatically align the needle guide and lock in place.
9. Manually insert the needle along prescribed axis as virtual needle guide is displayed on real-time MR images intersecting the needle axis.
10. Confirm correct placement.
11. Harvest tissue or deliver therapy.
12. Retract the needle guide and remove biopsy or brachytherapy needle from robot.

13. Update surgical plan as necessary based on volumetric imaging of the prostate and knowledge of the intervention performed.
14. Repeat for as many needles as necessary.

6.4 Teleoperated Needle Insertion

Manual insertion was the preferred technique due to the need for tactile feedback during the insertion phase. However, it was found that the ergonomics of manual insertion along this guide proved very difficult in the confines of the scanner bore. The limited space in closed-bore high-field MRI scanners requires a physical separation between the surgeon and the imaged region of the patient. To overcomes the loss of needle tip proprioception information, we are developing a teleoperated haptic system with optical force-torque sensor, to be integrated with a 3-DOF robotic needle driver for MR-guided prostate needle placement. The piezoelectrically actuated robot incorporates tactile feedback and teleoperation. As shown in Fig. 12, an MRI compatible robot controller sits inside the scanner room and communicates to the navigation software and scanner interface running on a laptop in the console room through a fiber optic connection. The optical force sensor interface is incorporated into the in-room robot controller and the needle interaction forces are transmitted back to the navigation software console along with the robot position. The haptic feedback device is integrated into the navigation software framework to provide forces to the operator and control back to the robot.

A direct force feedback architecture [6] is used to control the teleoperated needle placement system. In this iteration of the system, a commercially available Novint Falcon (Novint Technologies, Inc., Albuquerque, NM) haptic device is used as the master robot. It has 3 position DOF and can be used to position the needle in the Cartesian space. Other high quality haptic devices [28] can be utilized to enhance the teleoperation fidelity. In the future version, the haptic device would be designed with piezoelectric actuation and optical encoding as shown in Fig. 12. It would be operated inside the scanner room for better observation of patient's physiological condition and other surgical procedures. The human operator positions obtained from the haptic interface are used for trajectory generation and control of the motion of the slave manipulator. The slave robot in this design is the second generation of the 2-DOF pneumatically actuated robotic assistant system which overcomes many design difficulties and promises safe and reliable intraprostatic needle placement inside closed high-field MRI scanners. However, the addition of force feedback allows incorporation of an actuated needle driver and firing mechanism with needle rotation. The contact forces between needle and the tissue can be measured by the force/toque sensor [41, 45] and further fed back to the haptic device through its interface.

7 Experiments

The first iteration of the needle placement robots has been constructed and is operational. All mechanical, electrical, communications and software issues have been evaluated. The current state of the pneumatic manipulator is two actuated DOFs (vertical and horizontal) with an encoded passive needle insertion stage. Evaluation

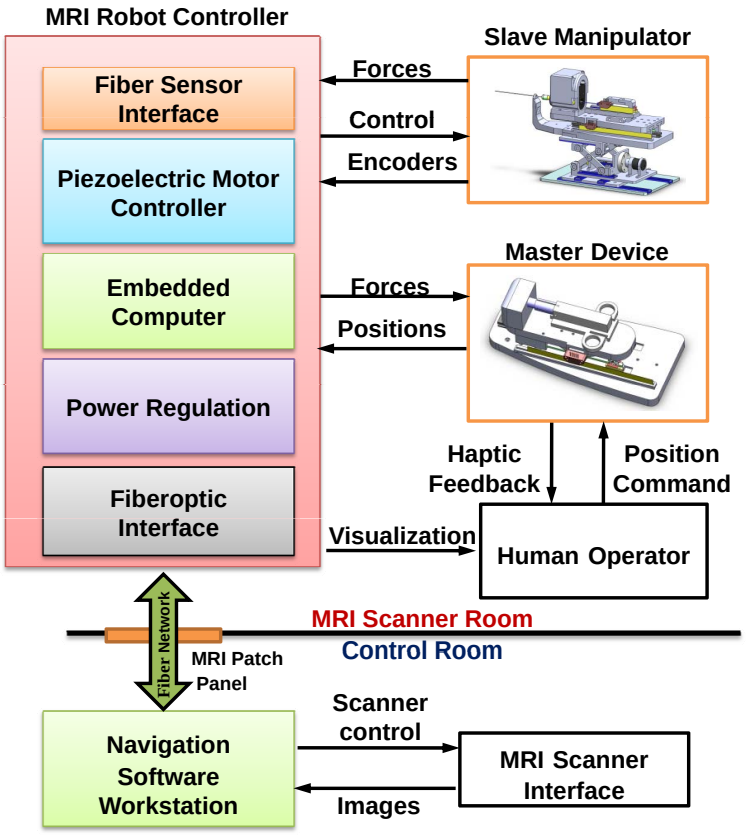

Fig. 12. System architecture for the master - slave haptic interface of the piezoelectric robot. The fiber optic force sensor and robot are placed near the isocenter of the MRI scanner, the master manipulator is connected to the navigation software interface, and the two are couple through the robot controller in the scanner room using a fiber optic network connection.

of the robot is in two distinct phases: 1) evaluation of the MR compatibility of the robot; and 2) evaluation of the workspace and accuracy. The piezoelectric actuated robot is 6-DOF and the MRI compatibility has been evaluated using similar protocols. This section reports the experimental setup and results of the two robots.

7.1 Imaging Protocols

Four imaging protocols as shown in Table 1, were selected for evaluation of compatibility of the system: 1) diagnostic imaging T1-weighted fast gradient echo (T1 FGE/FFE), 2) diagnostic imaging T2-weighted fast spin echo (T2 FSE/TSE), 3) high-speed real-time imaging fast gradient echo (FGRE), and 4) functional imaging spin echo-planar imaging (SE EPI). Details of the scan protocols are shown in

Table 1. All sequences were acquired with a slice thickness of 5mm and a number of excitations (NEX) of one. Three configurations were evaluated and used in the comparison: 1) baseline of the phantom only, 2) motor powered with controllers DC power supply turned on and 3) system servoing inside MRI board. Three slices were acquired per imaging protocol for each configuration.

Table 1. Scan Parameters for Compatibility Evaluation – 3T Philips Achieva

Protocol	**FOV**	**TE**	**TR**	**Flip Ang**	**Bandwidth**
T1W	240 mm	2.3 ms	225 ms	75^o	751 Hz/pixel
T2W	240 mm	90 ms	3000 ms	90^o	158 Hz/pixel
FGRE	240 mm	2.1 ms	6.4 ms	50^o	217 Hz/pixel
EPI	240 mm	45 ms	188 ms	90^o	745 Hz/pixel

Compatibility was evaluated on a 3T Philips Achieva scanner. A 110 mm, fluid-filled spherical MR phantom was placed in the isocenter and the robot placed such that the tip was at a distance of 120 mm from the center of the phantom (a representative depth from perineum to prostate), as shown in Fig. 4(right). For the pneumatic robot, the phantom was imaged using four standard prostate imaging protocols: 1) T1W FFE: T1 weighted fast field gradient echo; 2) T2W TSE: T2 weighted turbo spin echo; 3) TFE (FGRE): "real-time" turbo field gradient echo.

A baseline scan with each sequence was taken of the phantom with no robot components using round flex coils similar to those often used in prostate imaging. The following imaging series were taken in each of the following configurations: 1) phantom only; 2) controller in room and powered; 3) robot placed in scanner bore; 4) robot electrically connected to controller; and 5) robot moving during imaging (only with T1W imaging). For each step, all three imaging sequences were performed and both magnitude and phase images were collected.

The amount of degradation of SNR was used as the measure of negative effects on image quality. SNR of the MR images was defined as the mean signal in a 25 mm square at the center of the homogeneous sphere divided by the standard deviation of the signal in that same region. The SNR was normalized by the value for the baseline image, thus limiting any bias in choice of calculation technique or location. SNR was evaluated at seven 3 mm thick slices (representing a 25 mm cube) at the center of the sphere for each of the three imaging sequences. When the robot was operational, the reduction in SNR of the cube at the phantom's center for these pulse sequences was 5.5% for T1W FFE, 4.2% for T2W TSE, and 1.1% for TFE (FGRE). Further qualitative means of evaluating the effect of the robot on image quality are obtained by examining prostate images taken both with and without the presence of the robot. Fig. 13 shows images of the prostate of a volunteer placed in the scanner bore on the leg rest. With the robot operational, there is no visually identifiable loss in image quality of the prostate.

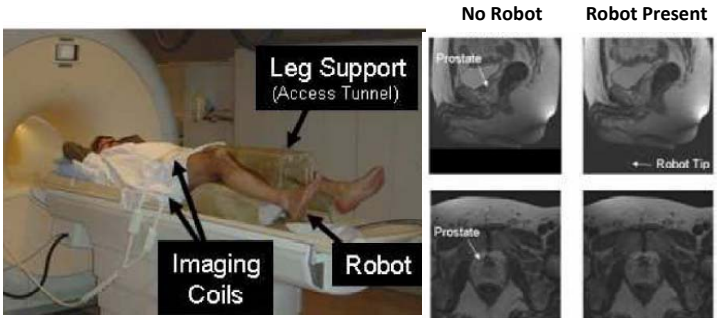

Fig. 13. Qualitative analysis of prostate image quality for pneumatic robot. Patient is placed on the leg support and the pneumatic robot sits inside of the support tunnel inside the scanner bore. T2 weighted sagittal and transverse images of the prostate taken when no robot components were present and when the robot was active in the scanner. [15] ©IEEE 2008

7.2 MR Compatibility of Pneumatic Actuated Needle Placement Robot

As can be seen in Fig. 13, the motors and encoders provide very small visually identifiable interference with the operation of the scanner. Fig. 15 depicts one slice of the tracking fiducial frame which provides the full position information of the robot. We utilize SNR as the metric for evaluating MR compatibility with baseline phantom image comparison. For comparison, the SNR of each configuration was normalized by the average SNR of the 3 baseline images for each imaging protocol. SNR of the MR images is defined as the mean signal in a 25mm square at the center of the homogeneous sphere divided by the standard deviation of the signal in that same region [53]. The SNR was normalized by the value for the baseline image. The technique used for measuring SNR is equivalent to that described by the NEMA standard [2]. The SNR is calculated as described in Method 4 of the cited standard:

$$SNR = \frac{S}{imagenoise} \tag{1}$$

where, S is the mean pixel value within the Measurement Region of Interest (MROI) and *imagenoise* is the standard deviation (SD) of the selected Noise Measurement Region of Interest (NMROI). The location of the NMROI has a significant impact on calculated SNR; the selected NMROI in the top-left corner minimizes variance between image slices and is outside of ghosting artifacts as described by Firbank, *et al* [14]. Statistical analysis with a Tukey Multiple Comparison confirms that no pair shows significant signal degradation with a 95% confidence interval.

7.3 Accuracy of Pneumatic Actuated Needle Placement Robot

Accuracy assessment is broken into two parts: localization and placement. These two must be distinguished, especially in many medical applications. In prostate

biopsy, it is essential to know exactly where a biopsy comes from in order to be able to form a treatment plan if cancer is located. In brachytherapy treatment, radioactive seed placement plans must be made to avoid cold spots where irradiation is insufficient; by knowing where seeds are placed, the dosimetry and treatment plan can be interactively updated. Based on encoder resolution, localization accuracy of the robot in free space is better than 0.1mm in all directions.

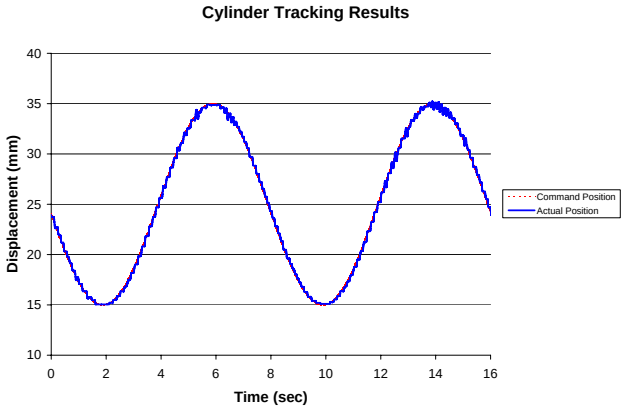

Fig. 14. Dynamic tracking results for the pneumatic cylinder for an 8sec period, 20mm amplitude sine wave.

Positioning accuracy is dependent on the servo pneumatic control system. The current control algorithm for pneumatic servo control is based upon sliding mode control techniques. The pneumatic cylinder was commanded to move back and forth between two points and the steady state error for each move was recorded. The average positioning accuracy was 0.26mm RMS error. In addition to point-to-point moves, the positioning accuracy of the cylinder alone in free space has been evaluated for dynamic trajectory tracking. The cylinder was commanded to follow a 0.125Hz, 20mm amplitude sine wave. Fig. 14 shows the tracking results for the cylinder. The RMS error for this task was 0.23mm which approximates the set deadband of 0.30mm.

7.4 MR Compatibility of Piezoelectric Actuated Needle Placement Robot

The four imaging protocols shown in Table 1 were evaluated in the same setup and the same metric (SNR). As can be seen in Fig. 15 (left), the motors and encoders provide very small visually identifiable interference with the operation of the scanner. Fig. 15 (right) depicts one slice of the tracking fiducial frame which provides the full position information of the robot. Statistical analysis with a Tukey Multiple Comparison confirms that no pair shows significant signal degradation with a 95% confidence interval. This result presents significant improvement over recent research

result in [26]. It implies that piezoelectric actuation is also feasible inside scanner bore during imaging, and thus makes it a good candidate in robotic design.

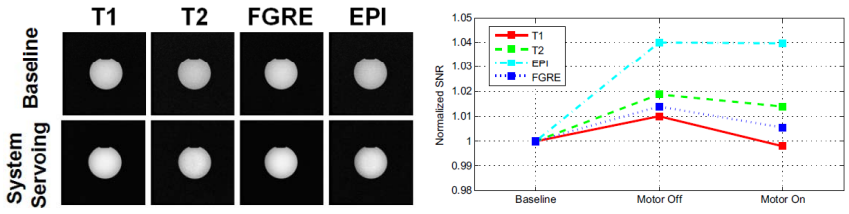

Fig. 15. Representative results showing the images obtained of baseline and system servoing inside scanner bore conditions (left), Results of the normalized SNR under each protocol. No statistically significant variations exist between baseline and motor running conditions (right).

8 Conclusions

This chapter presents two MRI-compatible approaches to image-guided transperineal prostate needle placement. Described is the mechanism, actuator and sensor design, controller design and system integration for a pneumatically actuated robotic needle guide and a piezoelectrically actuated needle steering platform. The 2-DOF pneumatic robot with manual needle insertion has an SNR loss limited to 5% with alignment accuracy under servo pneumatic control better than $0.94mm$ per axis. While the 6-DOF piezoelectrically actuated robot is the first demonstration of a novel multi piezoelectric actuator drive with less than 2% SNR loss for high field MRI operating at full speed during imaging. The preliminary experiments in phantom studies evaluate system MRI compatibility, workflow, visualization and targeting accuracy.

Attaining an acceptable level of MR compatibility required significant experimental evaluation. Several types of actuators, including piezoelectric motors and pneumatic cylinder/valve pairs, were evaluated. Pneumatic actuators have great potential for MRI-compatible mechatronic systems. Since no electronics are required, they are fundamentally compatible with the MR environment. However, there are several obstacles to overcome. These include: 1) material compatibility that was overcome with custom air cylinders made of glass with graphite pistons; 2) lack of stiffness or instability that was overcome with the development of a pneumatic brake that locks the cylinder's rod during needle insertion; and 3) difficult control that was ameliorated by using high-speed valves and shortening pneumatic hose lengths by designing an MRI-compatible controller. Pneumatic actuation seems to be an ideal solution for this robotic system, and it allows the robot to meet all of the design requirements. Further, MR compatibility of the system including the robot and controller is excellent with no more than a 5% loss in average SNR with the robot operational.

The pneumatic and piezoelectric systems have been evaluated in a variety of tests. The MR compatibility has shown to be sufficient for anatomical imaging using traditional prostate imaging sequences. Communications between all of the elements, including the robot, the low level controller, the planning workstation, and the MR scanner real-time imaging interface, are in place. Initial phantom studies validated the workflow and the ability to accurately localize the robot and target a lesion.

The pneumatic actuation and piezoelectric actuation presents complementary advantages and disadvantages. Pneumatic actuation is considered as the "ultimate solution" for MRI applications in the sense that these system can completely get rid of electrical and magnetic fields by using dielectric materials. However, due to the promising result implemented in the piezoelectric robot and the scalability, simplicity, size and inherent robustness of electromechanical systems present a clear advantage over pneumatically actuated systems. The piezoelectric actuation is considered as the rule of thumb actuation method that has been implemented as the slave robot presented here. A future development would be augmenting the slave robot to a teleoperated master-slave system. The slave robot would perform the needle placement under the surgeon motion command while the needle insertion force would be measured using the fiber optic force sensors that are being developed [39, 41, 43].

Acknowledgements

This work is supported in part by the Congressionally Directed Medical Research Programs Prostate Cancer Research Program (CDMRP PCRP) New Investigator Award W81XWH-09-1-0191 and Worcester Polytechnic Institute internal funds.

References

1. Standard test method for measurement of magnetically induced displacement force on passive implants in the magnetic resonance environment, F2052, vol. 13.01. American Society for Testing and Materials (ASTM) (2002)
2. Determination of Signal-to-Noise Ratio (SNR) in Diagnostic Magnetic Resonance Imaging, NEMA Standard Publication MS 1-2008. The Association of Electrical and Medical Imaging Equipment Manufacturers (2008)
3. Blumenfeld, P., Hata, N., Dimaio, S., Zou, K., Haker, S., Fichtinger, G., Tempany, C.: Transperineal prostate biopsy under magnetic resonance image guidance: A needle placement accuracy study **26**(3), 688–694 (2007)
4. Bone, G., Ning, S.: Experimental comparison of position tracking control algorithms for pneumatic cylinder actuators. IEEE/ASME Transactions on Mechatronics **12**(5), 557–561 (2007)
5. van den Bosch, M.R., Moman, M.R., van Vulpen, M., Battermann, J.J., Duiveman, E., van Schelven, L.J., de Leeuw, H., Lagendijk, J.J.W., Moerland, M.A.: MRI-guided robotic system for transperineal prostate interventions: proof of principle. Physics in Medicine and Biology **55**(5), N133 (2010)
6. Cavusoglu, M.C., Sherman, A., Tendick, F.: Design of bilateral teleoperation controllers for haptic exploration and telemanipulation of soft environments. IEEE Transactions on Robotics and Automation **18**(4), 641 – 647 (2002)

7. Chinzei, K., Miller, K.: Towards MRI guided surgical manipulator. Med Sci Monit **7**(1), 153–163 (2001)
8. Cole, G., Harrington, K., Su, H., Camilo, A., Pilitsis, J., Fischer, G.: Closed-loop actuated surgical system utilizing real-time in-situ MRI guidance. In: 12th International Symposium on Experimental Robotics - ISER 2010. New Delhi and Agra, India (2010)
9. Cole, G., Harrington, K., Su, H., Camilo, A., Pilitsis, J., Fischer, G.: Closed-loop actuated surgical system utilizing real-time in-situ MRI guidance. In: O. Khatib, V. Kumar, G. Sukhatme (eds.) Experimental Robotics, Springer Tracts in Advanced Robotics. Springer-Verlag (2011)
10. D'Amico, A.V., Cormack, R., Tempany, C.M., Kumar, S., Topulos, G., Kooy, H.M., Coleman, C.N.: Real-time magnetic resonance image-guided interstitial brachytherapy in the treatment of select patients with clinically localized prostate cancer. Int J Radiat Oncol Biol Phys **42**(3), 507–515 (1998)
11. DiMaio, S.P., Pieper, S., Chinzei, K., Hata, N., Haker, S.J., Kacher, D.F., Fichtinger, G., Tempany, C.M., Kikinis, R.: Robot-assisted needle placement in open MRI: system architecture, integration and validation. Comput Aided Surg **12**(1), 15–24 (2007)
12. Elhawary, H., Zivanovic, A., Davies, B., Lamperth, M.: A review of magnetic resonance imaging compatible manipulators in surgery. Proc Inst Mech Eng H **220**(3), 413–424 (2006)
13. Elhawary, H., Zivanovic, A., Rea, M., Davies, B., Besant, C., McRobbie, D., de Souza, N., Young, I., Lamperth, M.: The Feasibility of MR-Image Guided Prostate Biopsy Using Piezoceramic Motors Inside or Near to the Magnet Isocentre. In: R. Larsen, M. Nielsen, J. Sporring (eds.) Medical Image Computing and Computer-Assisted Intervention MICCAI 2006, *Lecture Notes in Computer Science*, vol. 4190, pp. 519–526. Springer Berlin Heidelberg
14. Firbank, M.J., Coulthard, A., Harrison, R.M., Williams, E.D.: A comparison of two methods for measuring the signal to noise ratio on mr images. Phys Med Biol **44**(12), N261–N264 (1999)
15. Fischer, G., Iordachita, I., Csoma, C., Tokuda, J., DiMaio, S., Tempany, C., Hata, N., Fichtinger, G.: MRI-compatible pneumatic robot for transperineal prostate needle placement. Mechatronics, IEEE/ASME Transactions on **13**(3), 295 –305 (2008)
16. Fischer, G.S., Su, H.: Apparatus and methods for MRI-compatible haptic interface. PCT International Patent Application: PCT/US10/56020 (2010)
17. Fu, L., Liu, H., Ng, W.S., Rubens, D., Strang, J., Messing, E., Yu, Y.: Hybrid dosimetry: feasibility of mixing angulated and parallel needles in planning prostate brachytherapy. Med Phys **33**(5), 1192–1198 (2006)
18. Futterer, J.J., Misra, S., Macura, K.J.: MRI of the prostate: potential role of robots. Imaging in Medicine **2**(5), 583–592 (2010)
19. Gassert, R., Dovat, L., Lambercy, O., Ruffieux, Y., Chapuis, D., Ganesh, G., Burdet, E., Bleuler, H.: A 2-dof fMRI compatible haptic interface to investigate the neural control of arm movements. Proceedings. 2006 Conference on International Robotics and Automation, pp. 3825–31. IEEE, Piscataway, NJ, USA (2006)
20. Gassert, R., Yamamoto, A., Chapuis, D., Dovat, L., Bleuler, H., Burdet, E.: Actuation Methods for Applications in MR Environments. Concepts in Magnetic Resonance Part B: Magnetic Resonance Engineering **29B**(4), 191–209 (2006)

21. Goldenberg, A., Trachtenberg, J., Kucharczyk, W., Yi, Y., Haider, M., Ma, L., Weersink, R., Raoufi, C.: Robotic system for closed-bore MRI-guided prostatic interventions. Mechatronics, IEEE/ASME Transactions on **13**(3), 374 –379 (2008)
22. Haker, S.J., Mulkern, R.V., Roebuck, J.R., Barnes, A.S., Dimaio, S., Hata, N., Tempany, C.M.: Magnetic resonance-guided prostate interventions. Top Magn Reson Imaging **16**(5), 355–368 (2005)
23. Huang, H., Su, H., Chen, H., K., M.J.: Piezoelectric driven non-toxic injector for automated cell manipulation. In: Proceedings of MMVR18 (Medicine Meets Virtual Reality). Newport Beach, California, USA (2011)
24. Huang, H., Sun, D., Su, H., Mills, J.: Force sensing and control of robot-assisted cell injection. In: T. Gulrez, A. Hassanien (eds.) Advances in Robotics and Virtual Reality. Springer-Verlag (2011)
25. Jemal, A., Siegel, R., Ward, E., Hao, Y., Xu, J., Thun, M.J.: Cancer statistics, 2009. CA Cancer J Clin **59**(4), 225–249 (2009)
26. Krieger, A., Iordachita, I., Song, S.E., Cho, N., Guion, P., Fichtinger, G., Whitcomb, L.: Development and preliminary evaluation of an actuated MRI-compatible robotic device for MRI-guided prostate intervention. In: Robotics and Automation (ICRA), 2010 IEEE International Conference on, pp. 1066 – 1073 (2010)
27. Krieger, A., Susil, R.C., Meard, C., Coleman, J.A., Fichtinger, G., Atalar, E., Whitcomb, L.L.: Design of a novel MRI compatible manipulator for image guided prostate interventions. IEEE Trans Biomed Eng **52**(2), 306–313 (2005)
28. Lee, L., Narayanan, M.S., Mendel, F., Krovi, V.N.: Kinematics analysis of in-parallel 5 dof haptic device. In: 2010 IEEE/ASME International Conference on Advanced Intelligent Mechatronics. Montreal, Canada (2010)
29. Li, M., Kapoor, A., Mazilu, D., Horvath, K.A.: Pneumatic actuated robotic assistant system for aortic valve replacement under MRI guidance. IEEE Transactions on Biomedical Engineering **58**(2), 443–451 (2010)
30. Li, M., Mazilu, D., Horvath, K.A.: Robotic system for transapical aortic valve replacement with MRI guidance. In: Proceedings of the 11th International Conference on Medical Image Computing and Computer-Assisted Intervention, Part II, pp. 476–484. Springer-Verlag, Berlin, Heidelberg (2008)
31. Masamune, K., Kobayashi, E., Masutani, Y., Suzuki, M., Dohi, T., Iseki, H., Takakura, K.: Development of an MRI-compatible needle insertion manipulator for stereotactic neurosurgery. J Image Guid Surg **1**(4), 242–248 (1995)
32. Melzer, A., Gutmann, B., Remmele, T., Wolf, R., Lukoscheck, A., Bock, M., Bardenheuer, H., Fischer, H.: Innomotion for percutaneous image-guided interventions. Engineering in Medicine and Biology Magazine, IEEE **27**(3), 66 –73 (2008)
33. Mewes, P., Tokuda, J., DiMaio, S.P., Fischer, G.S., Csoma, C., Gobi, D.G., Tempany, C., Fichtinger, G., Hata, N.: An integrated MRI and robot control software system for an MR-compatible robot in prostate intervention. In: Proc. IEEE International Conference on Robotics and Automation ICRA 2008 (2008)
34. Pondman, K.M., Futerer, J.J., ten Haken, B., Kool, L.J.S., Witjes, J.A., Hambrock, T., Macura, K.J., Barentsz, J.O.: MR-guided biopsy of the prostate: An overview of techniques and a systematic review. European Urology **54**(3), 517 – 527 (2008)
35. Schouten, M.G., Ansems, J., Renema, W.K.J., Bosboom, D., Scheenen, T.W.J., Futterer, J.J.: The accuracy and safety aspects of a novel robotic needle guide

manipulator to perform transrectal prostate biopsies. Medical Physics **37**(9), 4744–4750 (2010)
36. Shellock, F.G.: Magnetic resonance safety update 2002: implants and devices. J Magn Reson Imaging **16**(5), 485–496 (2002)
37. Song, S.E., Cho, N.B., Fischer, G., Hata, N., Tempany, C., Fichtinger, G., Iordachita, I.: Development of a pneumatic robot for MRI-guided transperineal prostate biopsy and brachytherapy: New approaches. In: Proc. IEEE International Conference on Robotics and Automation ICRA (2010)
38. Stoianovici, D., Patriciu, A., Petrisor, D., Mazilu, D., Kavoussi, L.: A new type of motor: pneumatic step motor. IEEE/ASME Transactions on Mechatronics **12**(1), 98–106 (2007)
39. Su, H., Camilo, A., Cole, G., Hata, N., Tempany, C., Fischer, G.: High-field MRI compatible needle placement robot for prostate interventions. In: Proceedings of MMVR18 (Medicine Meets Virtual Reality). Newport Beach, California, USA (2011)
40. Su, H., Cole, G., Fischer, G.: Active needle steering for percutaneous prostate intervention in high-field MRI. In: 2010 Robotics: Science and Systems Conference, Workshop on Enabling Technologies for Image-Guided Robotic Interventional Procedures. Zaragoza, Spain (2010)
41. Su, H., Fischer, G.S.: A 3-axis optical force/torque sensor for prostate needle placement in magnetic resonance imaging environments. In: 2nd Annual IEEE International Conference on Technologies for Practical Robot Applications. IEEE, Boston, MA, USA (2009)
42. Su, H., Harrington, K., Cole, G., Wang, Y., Fischer, G.: Modular needle steering driver for MRI-guided transperineal prostate intervention. In: IEEE International Conference on Robotics and Automation, Workshop on Snakes, Worms and Catheters: Continuum and Serpentine Robots for Minimally Invasive Surgery. Anchorage, AK, USA (2010)
43. Su, H., Shang, W., Cole, G., Harrington, K., Gregory, F.S.: Haptic system design for MRI-guided needle based prostate brachytherapy. IEEE Haptics Symposium 2010. IEEE, Boston, MA, USA (2010)
44. Su, H., Zervas, M., Cole, G., Furlong, C., Fischer, G.: Real-time MRI-guided needle placement robot with integrated fiber optic force sensing. In: IEEE ICRA 2011 International Conference on Robotics and Automation. Shanghai, China (2011)
45. Su, H., Zervas, M., Furlong, C., Fischer, G.S.: A miniature MRI-compatible fiber-optic force sensor utilizing Fabry-Perot interferometer. MEMS and Nanotechnology, Conference Proceedings of the Society for Experimental Mechanics Series, pp. 131–136 (2011)
46. Sutherland, G.R., Latour, I., Greer, A.D., Fielding, T., Feil, G., Newhook, P.: An image-guided magnetic resonance-compatible surgical robot. Neurosurgery **62**(2), 286–92; discussion 292–3 (2008)
47. Suzuki, T., Liao, H., Kobayashi, E., Sakuma, I.: Ultrasonic motor driving method for EMI-free image in MR image-guided surgical robotic system. In: Proc. IEEE/RSJ International Conference on Intelligent Robots and Systems IROS 2007, pp. 522–527 (2007)
48. Terris, M.K., Wallen, E.M., Stamey, T.A.: Comparison of mid-lobe versus lateral systematic sextant biopsies in the detection of prostate cancer. Urol Int **59**(4), 239–242 (1997)

49. Tokuda, J., Fischer, G.: OpenIGTLink: an open network protocol for image-guided therapy environment. Int J Med Robot **5**(4), 423–34 (2009)
50. Tokuda, J., Fischer, G.S., DiMaio, S.P., Gobbi, D.G., Csoma, C., Mewes, P.W., Fichtinger, G., Tempany, C.M., Hata, N.: Integrated navigation and control software system for MRI-guided robotic prostate interventions. Computerized Medical Imaging and Graphics **34**(1), 3 – 8 (2010)
51. Tsekos, N.V., Khanicheh, A., Christoforou, E., Mavroidis, C.: Magnetic resonance-compatible robotic and mechatronics systems for image-guided interventions and rehabilitation: a review study. Annu Rev Biomed Eng **9**, 351–387 (2007)
52. Wallner, K., Blasko, J., Dattoli, M.: Prostate Brachytherapy Made Complicated, 2nd Ed. SmartMedicine Press (2001)
53. Wang, Y., Cole, G., Su, H., Pilitsis, J., Fischer, G.: MRI compatibility evaluation of a piezoelectric actuator system for a neural interventional robot. In: Annual Conference of IEEE Engineering in Medicine and Biology Society, pp. 6072–6075. Minneapolis, MN (2009)
54. Wang, Y., Su, H., Harrington, K., Fischer, G.: Sliding mode control of piezoelectric valve regulated pneumatic actuator for MRI-compatible robotic intervention. In: ASME Dynamic Systems and Control Conference - DSCC 2010. Cambridge, Massachusetts, USA (2010)
55. Webster R.J., I., Kim, J.S., Cowan, N., Chirikjian, G., Okamura, A.: Nonholonomic modeling of needle steering. International Journal of Robotics Research **25**(5-6), 509 –25 (2006)
56. Yang, B., Tan, U., Gullapalli, R., McMillan, A., Desai, J.: Design and implementation of a pneumatically-actuated robot for breast biopsy under continuous MRI. In: IEEE ICRA 2011 International Conference on Robotics and Automation. Shanghai, China (2011)
57. Yeniaras, E., Lamaury, J., Hedayati, Y., Sternberg, N.V., Tsekos, N.V.: Prototype cyber-physical system for magnetic resonance based, robot assisted minimally invasive intracardiac surgeries. International Journal of Computer Assisted Radiology and Surgery (2011)

Index